第37卷,第12期 光 谱 学 与 光 谱 分 析 Vol. 37, No. 12, pp3932-3939
2017年12月 Spectroscopy and Spectral Analysis December, 2017

A Stepped Mirror Based Temporally and Spatially Modulated Imaging Fourier Transform Spectrometer: Principle and Data Processing

GAO Jian-hua[1,2], LIANG Jing-qiu[1], LÜ Jin-guang[1]*, LIANG Zhong-zhu[1], QIN Yu-xin[1], WANG Wei-biao[1]

1. State Key Laboratory of Applied Optics, Changchun Institute of Optics, Fine Mechanics and Physics, Chinese Academy of Sciences, Changchun 130033, China
2. University of Chinese Academy of Sciences, Beijing 100049, China

Abstract This manuscript introduces the principle and data processing method of a stepped mirror based temporally and spatially modulated imaging Fourier transform spectrometer. The instrument substitutes the moving mirror, which is widely used in a Michelson interferometer, with a stepped mirror to realize static interference. A scanning mirror is placed in front of the first imaging system to make the target image on different sub-mirrors to get different optical path differences. Light emitted from the target propagate through the scanning mirror and the first imaging system to focus on the stepped mirror and the plane mirror to form two primary images. The primary images are then reflected by the stepped and plane mirrors to propagate through the second imaging system and finally image on the detector. Since there are optical path differences between the stepped mirror and the plane mirror, the image captured by the detector would have the two-dimensional spatial and one-dimensional spectral information of the target. The scanning interval of the scanning mirror is set to be 0.095° according to the parameters of the stepped mirror and the optical system. Image stitching and spectrum reconstruction are done using the experimental data cube. A polar Hough transform based image cutting method is proposed to deal with the sub-mirror width difference problem in image cutting. To mitigate the discontinuity line effect in the panorama, the image is transformed to the HSI space to adjust its intensity. After interferogram dimension reduction, direct current offset removal, interferogram addressing, apodization, phase correction, Fourier transform and spectral resolution enhancement, the spectrum is reconstructed and its resolution is 194 cm^{-1}, which is better than the designed value (250 cm^{-1}).

Keywords Imaging Fourier transform spectrometer; Interferogram stitching; Spectrum reconstruction; Image stitching

中图分类号: TH74 **文献标识码**: A **DOI**: 10.3964/j.issn.1000-0593(2017)12-3932-08

Received: 2017-01-06; **accepted**: 2017-05-20

Foundation item: National Natural Science Foundation of China (61376122, 61627819, 61575193), Science and Technology Development Plan of Jilin Province (20150520101JH, 20150101049JC, 20150204072GX, 20170204077GX), Youth Innovation Promotion Association of CAS (2014193) and State Key Laboratory of Applied Optics, Changchun Institute of Optics, Fine Mechanics and Physics, Chinese Academy of Sciences

Biography: GAO Jian-hua, (1990—), a doctoral student at Changchun Institute of Optics, Fine Mechanics and Physics, Chinese Academy of Sciences e-mail: hitgaojianhua@163.com *Corresponding author e-mail: jinguanglv@163.com

Introduction

Many noxious gases and volatile organic compounds (VOCs) have absorption peaks in the mid-infrared, for example, SO_2 has an absorption peak at 4 μm, CO at 4.8 μm, HCHO (formaldehyde) at 3.6 μm. In case of an emergency such as a fire explosion, the leakage of noxious gases or VOCs can lead to devastating consequences. Therefore, it is very necessary to pre-determine the type gases and VOCs and the location of leak sources in emergencies.

The imaging Fourier transform spectrometer (IFTS) can simultaneously acquire the two-dimension (2D) spatial information and one-dimension (1D) spectral information of the object by remote measurement. The spectral and spatial information can be used to find the type and location of the dangerous goods in emergencies.

According to the way the optical path difference (OPD) is produced, the IFTS can be classified into three types, temporally modulated, spatially modulated and temporally and spatially modulated[1]. The temporally modulated IFTS (TMIFTS) can reach a high spectral resolution but it needs precise motion control system to guarantee the accuracy of the OPDs. The spatially modulated IFTS (SMIFTS) removes the moving mirror away and thus realized the goal of a static interference system. However, the spatially modulated IFTS has a slit in the optical system, which forces it to make a tradeoff between the spectral resolution and the luminous flux. The temporally and spatially modulated IFTS (TSMIFTS) has no moving mirror or slit, and thus has the advantage of high luminous flux and static interfering.

Many kinds of TSMIFTS structures, such as the Savart plant based[2], the corner mirror based[3], the Sagnac based[4] and the scanning mirror based[5] have been proposed for different applications. In recent years, researchers proposed the snap shot imaging spectrometer (SSIS), which could capture the spatial and spectral information in a signal image and thus make the data capture process faster[6-8]. However, there are problems, such as the tradeoff between the spatial and spectral resolution, for the SSIS to overcome.

In 2015, Wang et. al proposed a stepped mirror based TSMIFTS, which could be used in emergency or environment monitor in the mid-infrared[9]. The stepped mirror based TSMIFTS has no slit or scanning mirror in the interference system, which brings it the advantage of multi-channels and high luminous flux.

The data processing method of IFTS has been investigated in many aspects[10-11], however, because of the unique structure of the stepped mirror, some part of the data processing is different from others. We have discussed the spectrum reconstruction of a stepped mirror based spatially modulated Fourier transform spectrometer (SMFTS) in[12]. In this paper, we will discuss the principle and data processing of a stepped mirror based TSMIFTS. Especially, the interferogram dimension reduction, nonuniform sample correction, and spectral resolution enhancement, which are different from the stepped mirror based on SMFTS, will be discussed in the spectrum reconstruction part.

1 Principles of the stepped mirror based TSMIFTS

1.1 The working principle

As shown in figure 1, the stepped mirror based TSMIFTS is composed of the scanning mirror, the first imaging system, the beam splitter, the compensating plate, the plane mirror, the stepped mirror, the second imaging system and the detector. Light emitted from the target propagate through the scanning mirror and the first imaging system to image on the stepped mirror and the plane mirror to form two primary images. The primary images are then reflected by the stepped and plane mirrors to propagate through the second imaging system and finally image on the detector. Since there are OPDs between the stepped mirror and the plane mirror, the image captured by the detector would have the spatial and spectral information of the target. By controlling the scanning mirror, the target could image on different sub-mirrors of the stepped mirror, and after a scanning period, we can get the data cube contains the spatial and spectral information of the target.

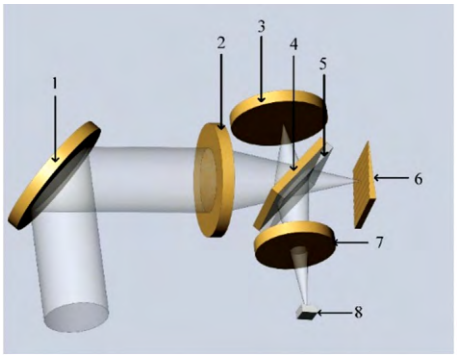

Fig. 1 Simplified configuration of the temporally and spatially modulated IFTS

1: Scanning mirror; 2: First imaging system; 3: Plane mirror; 4: Beam splitter; 5: Compensating plate; 6: Stepped mirror; 7: Second imaging system; 8: Detector

1.2 Sampling the interferogram

The stepped mirror is manufactured by micro-optical electromechanical system (MOEMS) technology, table 1 shows the parameters of the stepped mirror.

Table 1 Parameters of the stepped mirror

step height difference/μm	0.625
number of steps	32
total height/μm	20
width/mm	1
length/mm	32

Suppose the step height difference of the stepped mirror is H, the number of sub-mirrors is N. The position of the stepped mirror and the plane mirror is adjusted to make the OPD between the ith step and the plane mirror zero so that the space sampling interval is $2H$. Let the light wavelength range be $[\lambda_{min}, \lambda_{max}]$, where λ_{min} and λ_{max} indicate the minimum and maximum wavelengths that can be detected by the detector array, respectively.

According to the Nyquist-Shannon criterion, the sampling frequency f_s should satisfy $f_s \geqslant 2f_{max}$. The spatial sampling interval should therefore satisfy $2H \leqslant \lambda_{min}/2$, which means the height of one step of the stepped mirror should be equal to or less than $\lambda_{min}/4$.

1.3 Spectral resolution

The spectral resolution of IFTS could be described by its full width at half height (FWHH)

$$\mathrm{FWHM} = \frac{10\ 000}{\delta_{max}}\ \mathrm{cm}^{-1} \tag{1}$$

Where δ_{max} indicate the maximum OPD and its unit is micrometer.

1.4 Calculation of the scanning interval

To capture the interferogram of the target from zero OPD (ZPD) to its maximum OPD, the distance that the target moves on the stepped mirror should be less than or equal to the width of one sub-mirror. In practice, for the purpose of reducing the scanning time, the distance is set to be equal to the width of one sub-mirror.

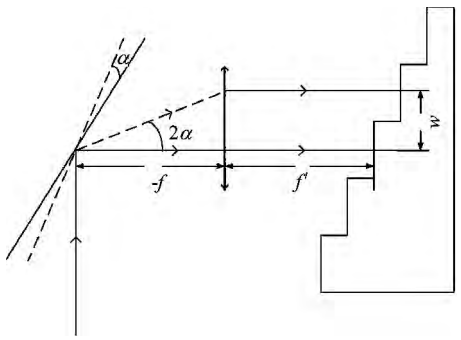

Fig. 2 Diagram of the scanning process from a sub-mirror to the adjacent one

As shown in figure 2, the principle ray propagates through the scanning mirror and the first imaging system to the stepped mirror. The focal length of the first imaging system is f', $-f=f'$, the width of one sub-mirror is w, the rotary angle of the scanning mirror is α, we can get

$$\tan(2\alpha) = \frac{w}{f'} \tag{2}$$

therefore,

$$\alpha = \frac{1}{2}\arctan\left(\frac{w}{f'}\right) \tag{3}$$

Since there is height difference between the sub-mirrors of the stepped mirror, there should be a certain amount of defocus in the first imaging system, which would bring disturbance to the rotary angle. Suppose the defocusing amount of the ith step is zero, then the defocusing amount of the $(i+n)$th sub-mirror should be $n\times H$, the rotary angle of the $(i+n)$th sub-mirror should be

$$\alpha_n = \frac{1}{2}\arctan\left(\frac{w}{f'+nH}\right) \tag{4}$$

In practice, the focal length of the first imaging system is 300 mm, the maximum defocusing amount is 19.375 μm, which is only 0.006% the focal length. Therefore, it is reasonable to ignore the defocusing amount and calculate the rotary angel by Eq. (3).

2 Data processing principles

After a scanning period, the data cube of the target is captured. Before image and spectrum stitching, the dark noise should be removed. Sheltering the entrance pupil to stop the radiation outside the instrument, the image captured by the detector is the dark image.

The images in a sub-mirror is defined as an image unit before cutting the images in the data cube into unit. Then comes to stitching the image units with the same target, but the interferogram of the target could be obtained from different OPDs in OPD order. Stitching the units with the same OPD in the scanning order could get the image in a scanning period.

2.1 Image cutting

The image cutting is the foundation of the successive process. Theoretically, the positions of different unit can be obtained by the geometry of the stepped mirror and the imaging of the aperture on the detector. However, because of the fabrication accuracy of the stepped mirror and the optical system alignment error, the width of different image unit may be different. Therefore, we applied the Hough transform to refine the positions of the image unit with respect to the predicted positions[13].

The Hough transform map the positions of the pixels from the coordinate space to the parameter space. The equation of a line passes through the point (x_i, y_i) in the Cartesian space could be written as:

$$y_i = ax_i + b \tag{5}$$

where a is the slope, b is the intercept.

There are numerous lines that passes through (x_i, y_i). If we set x_i and y_i as constant, a and b as variable, Eq. (5) could be written as

$$b = -ax_i + y_i \tag{6}$$

If two points are in the same line in the coordinate space, they should have same a and b in the parameter space.

Considering that the stepped mirror is placed vertically to the scanning direction, the slope of lines in the obtain images may be extremely big. Therefore, the pole coordinate is used instead of the Cartesian coordinate. The pole coordinate Hough transform could be written as

$$\rho = x\cos\theta + y\sin\theta \tag{7}$$

where ρ is the distance between the origin and the line, θ is the angle between the perpendicular of the line and the x axis.

2.2 Image stitching

As discussed above, stitching the units with the same OPD in time order could obtain the panorama in a scanning cycle. However, because of the light intensity difference in image units, the panorama would contain discontinuous lines if the image units are simply placed in a registration plane. Feature based method is applied to accomplish the image stitching, and it mainly contains feature point detection, feature description, feature matching and image fusion. To guarantee enough feature points could be detected, and the coincident ratio of the neighboring images is no less than 10%[14], the images used in stitching are bigger than an image unit.

2.2.1 Feature point detection

Feature points could be used to find the same object in different images. A typical feature point is the Harris corner point. The Harris corner point could be calculated by the following steps[15]:

1) Convolving the image with derivative of the horizontal and vertical Gaussian function.

$$\begin{aligned} I_x &= I * G'_x \\ I_y &= I * G'_y \end{aligned} \tag{8}$$

where I is the raw image, I_x and I_y are the horizontal and vertical derivative of I, G'_x and G'_y are the derivative of the horizontal and vertical Gaussian function, $*$ indicates convolution.

2) Calculate the eigenvalue of the following matrix

$$\begin{bmatrix} I_x^2 & I_x I_y \\ I_x I_y & I_y^2 \end{bmatrix} \tag{9}$$

3) Find the smallest eigenvalue in an area and the point corresponding to it is the feature point.

2.2.2 Feature description

Once the feature points are detected, it is necessary to find some descriptors to describe it. The scale invariant feature transform (SIFT) descriptor presented by Lowe et. al calculate the descriptor by computing the gradients of the points in a 16×16 window around the feature point[16]. The gradients are weighted by a Gaussian function to reduce the influence of the edge points.

2.2.3 Feature matching

After the feature descriptors are made, the Euclidean distance can be used in the feature space to match the feature points. A good strategy is to calculate the nearest neighbor distance ratio (NNDR) to accomplish the feature matching[17]. The smaller NNDR corresponding to the right matching. The NNDR is defined as:

$$\mathrm{NNDR} = \frac{d_1}{d_2} = \frac{\| D_A - D_B \|_2}{\| D_A - D_C \|_2} \tag{10}$$

where D_A is the descriptor of the target, D_B and D_C are the first two nearest neighbor of D_A, d_1 and d_2 are the Euclidean distance of ($D_A - D_B$) and ($D_A - D_C$).

2.2.4 Image fusion

Different sub-mirrors have different OPDs and thus make them have different light intensities. The target images to a sub-mirror at a certain moment, and the edge of the image unit would have sudden light intensity change, which would make the panorama contain discontinuity lines.

The method we used to deal with this problem is to transform the image to the HSI color space and adjust the I component. The main ideas behind this method is:

1) Transform the image to the HSI color space.

2) Substitute the intensity in the edge of the image unit with the one obtained by interpolation method.

2.3 Interferogram stitching and spectrum reconstruction

As discussed above, stitching the units with the same target but different OPD in OPD order could obtain the interferogram of the target. Once the interferogram is obtained, the spectrum could be reconstructed according to Eq. (11)

$$B(\sigma) = F\{I(\delta) - I_{dc}\} = \int_{-\infty}^{\infty} [I(\delta) - I_{dc}]\mathrm{e}^{-i2\pi\sigma\delta}\,\mathrm{d}\delta \tag{11}$$

where $B(\sigma)$ is the spectrum, $I(\delta)$ is the interferogram, I_{dc} is the direct current (DC) part of interferogram, and F indicates the Fourier transformation.

The spectrum reconstruction process including interferogram dimension reduction, DC offset removal, interferogram addressing, apodization, nonuniform sample correction, phase correction, Fourier transform and spectral resolution enhancement. The DC offset removal aims to remove the DC offset of the 1D interferogram. The interferogram addressing is to address the interferogram in OPD order. The effect of the apodization is to trade spectral resolution against oscillation in the line shape. The phase correction is to correct the random phase errors in the interferogram.

2.3.1 Interferogram stitching

The image units used in interferogram contain the same target, therefore, direct stitching method instead of the feature based method is used here. In detail, the image units ob-

tained by 3.1 are arranged to an image that has the same size with the image in the data cube.

2.3.2 Interferogram dimension reduction

The image should be transformed to 1D interferogram for the purpose of reconstructing the spectrum. Suppose the image in a sub-mirror is detected by n column pixels in the detector. The interferogram dimension reduction process could be described as Eq. 12 and Eq. 13:

$$\left(\begin{array}{ccc|c|ccc} I_{11} & \cdots & I_{1n} & \cdots & I_{1(N_t-n+1)} & \cdots & I_{1N_t} \\ I_{21} & & I_{1n} & \cdots & I_{1(N_t-n+1)} & & I_{1N_t} \\ \vdots & & \vdots & & \vdots & & \vdots \\ I_{M1} & \cdots & I_{Mn} & \cdots & I_{1(N_t-n+1)} & \cdots & I_{MN_t} \end{array}\right) \tag{12}$$

$$(I'_1 \quad I'_2 \quad \cdots \quad I'_N) \tag{13}$$

Where the rectangle area indicates an image unit, $N_t = N \times n$, $I'_i (i = 1, 2, \cdots, N)$ indicate the light intensity of the target with different OPDs.

2.3.3 Nonuniform sample correction

The height errors of the stepped mirrors would cause inherent errors in OPDs, which would seriously affect the accuracy of the reconstructed spectrum.

Table 2 Height test result of the stepped mirror

Maximum/nm	Minimum/nm	Mean/nm	Variance/nm
0.840	0.546	0.625	0.005

As we can see in table 2 the height of the stepped mirror drifted from the ideal value, which makes the sample interval nonuniform. According to P. Griffiths[18], the relationship between the maximum signal to noise ratio (SNR) and the sampling errors is

$$\mathrm{SNR}_{\max} = \frac{4}{\Delta x \tilde{\nu}_{\max}} \tag{14}$$

where Δx is the root-mean-square error (RMSE) of the sampling interval, $\tilde{\nu}_{\max}$ is the maximum wavenumber of the source.

If the SNR is higher than 1 000 at 4 000 cm^{-1}, Δx should within 10 nm, which is beyond the fabrication accuracy of the stepped mirrors. Therefore, the inherent OPD errors should be corrected before phase correction. Since the sampling interval error could be calculated from the tested step height, the interpolation method is used to correct the nonuniformity.

Define the height error as the tested value minus the ideal one. Suppose the height error of jth sub-mirror is Δ_j. The OPD error between the sub-mirror and the plane mirror should be

$$\delta E_j = 2 \times \Delta_j \tag{15}$$

Suppose $\delta R_i (i = 1, 2, \cdots, N)$ is the real OPD distribution, $\delta E_i (i = 1, 2, \cdots, N)$ is the error matrix, $\delta I_i (i = 1, 2, \cdots, N)$ is the ideal OPD distribution. After testing the step height of the stepped mirror, we can calculate the height deviation to the designed values. Then we can calculate δE_i and δR_i by Eq. (15) and Eq. (16)

$$\delta R_i = \delta I_i - \delta E_i \tag{16}$$

Once δR_i is obtained, the residual sampling error could be corrected by an interpolation method.

2.3.4 Spectral resolution enhancement

Since the spectral information is mainly in the high frequency part, we applied the empirical-mode decomposition (EMD) method to enhance the spectral resolution according to Eq. (17) and Eq. (18).

$$X(t) = \sum_{j=1}^{n} c_j(t) + r_n(t) \tag{17}$$

$$X(t) = \sum_{j=1}^{n} a_j c_j(t) + r'_n(t) \tag{18}$$

where $X(t)$ is the reconstructed signal, $c_j(t)$ is the intrinsic mode function (IMF) obtained by applying the EMD, a_j is the coefficient of $c_j(t)$, $r_n(t)$ and $r'_n(t)$ are the monotonic residue.

The IMF is identified by two characteristics: 1) the number of extrema and the number of zero crossings either be equal or differ at most by one in the whole data set, and 2) the mean value of the upper envelope defined by the local maxima and the lower envelope defined by the local minima should be equal to zero. To enhance the high frequency part of the spectrum doesn't means throw the low frequency part away, because the low frequency also contains some spectral information. The coefficient may be obtained by the process below:

1) Get maximum value M_j of each IMF_j, and calculate their algebraic sumS.

2) Calculate the initial coefficient b_j

$$b_j = \frac{M_j}{S} \tag{19}$$

3) Use an exponential function to calculate a_j

$$a_j = \begin{cases} b_1 + \Delta & j = 1 \\ \dfrac{b_j}{e^j} & j = 2, 3, \cdots, n \end{cases} \tag{20}$$

where $\Delta = \mathrm{sum}(b_j - a_j)$, $j = 2, 3, \cdots, n$, sum means the algebraic sum.

Once a_j is obtained, we can reconstruct the signal by Eq. (18).

3 Experiment results

Figure 3 shows the prototype of the stepped mirror based TSMIFTS, and some experiment have been performed with it at approximately 43°47′36″ north and 125°27′27″ east. The field of view of the system is ±4.31°. The scanning interval

is set as 0.095°. The step difference of the stepped mirror is 0.625 μm. The detector is a mercury cadmium telluride (MCT) mid-infrared plane detector array that contains 320×256 pixels with a pixel size of 30 μm×30 μm. Figure 4 shows four images in a data cube.

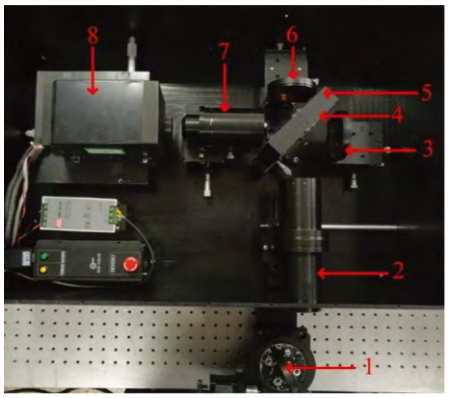

Fig. 3　Prototype of the stepped mirror based TSMIFTS

1: Scanning mirror; 2: First imaging system; 3: Plan mirror; 4: Beam splitter; 5: Compensating plate; 6: Stepped mirror; 7: Second imaging system; 8: Detector

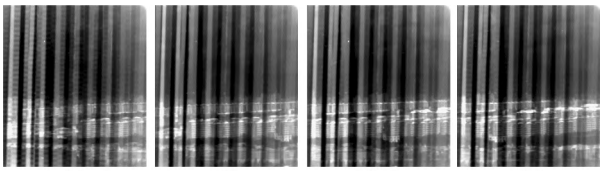

Fig. 4　(a) the first, (b) eleven, (c) twenty-two, and (d) thirty-two images in the data cube

Using the method discussed above, the image stitching and spectrum reconstruction have been accomplished. The panorama is shown in Figure 5 (a) and (b). The discontinuity line effect is corrected according to 3.2.4, and there is almost no discontinuity line in the rectangle area.

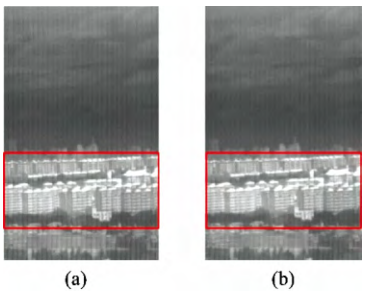

Fig. 5　Panoramas before (a) and after (b) the discontinuity line effect correct

The stitched interferogram is shown in Figure 6. Figure 7 (a) shows the 1D interferogram, with its base line (the red line) curved. Figure 7 (b) shows the interferogram after DC removal, as we can see, its base line is almost equals to zero.

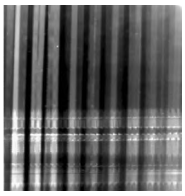

Fig. 6　Stitched interferogram

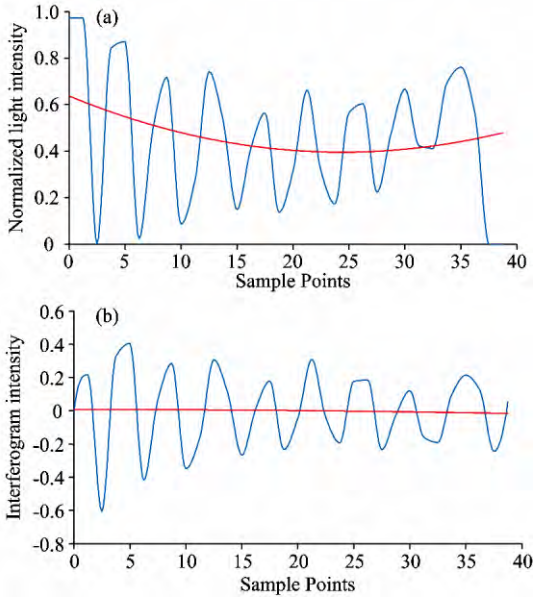

Fig. 7　(a) the 1D interferogram and its base line (the red line) and (b) the interferogram after DC removal and its base line (the red line)

The reconstructed spectrum is shown in Figure 8 (d). After the reconstructed by the EMD based method, the spectral resolution is enhanced from 307 to 194 cm^{-1}, which is better than the designed value (250 cm^{-1}).

4　Conclusion

The unique structure of the stepped mirror based temporally and spatially modulated IFTS not only owns the advantage of multi-channels and high luminous flux, but also makes its data processing method unique. Experiments results shows that the feature based stitching method could eliminate the slims caused by direct stitching, and adjust the intensity in the HSI space could mitigate the discontinuity line effect in the panorama. The spectral resolution is 194 cm^{-1}, which is better than the designed value. However, the spatial resolution is limited by the pixel number of the detector, which makes some part of the image unclear. Further efforts will be needed to enhance the spatial resolution of the image.

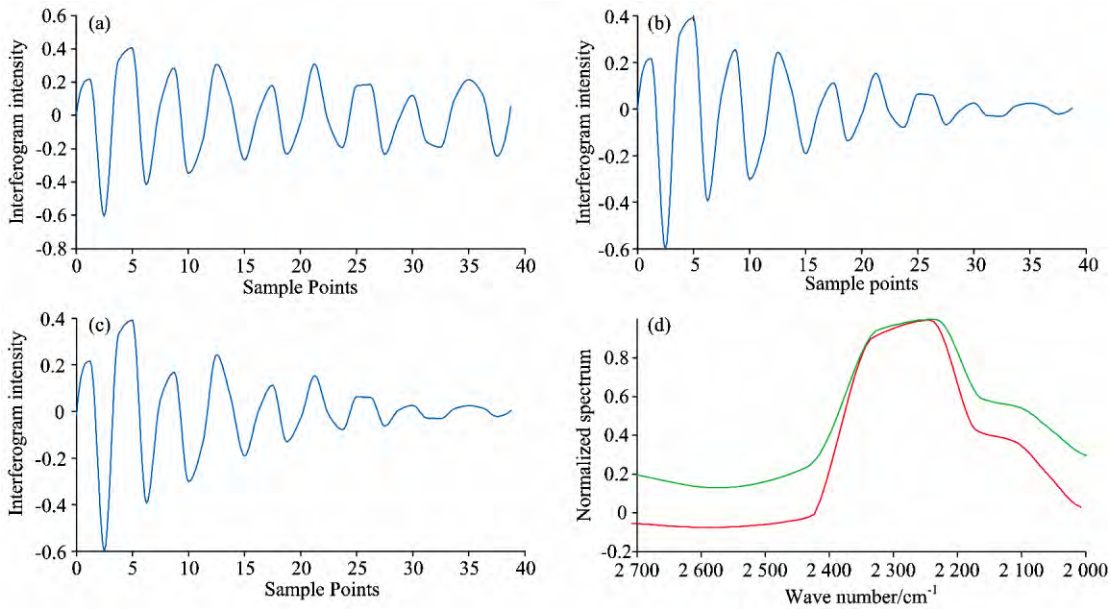

Fig. 8 (a) Interferogram after addressed in OPD order; (b) interferogram after apodization; (c) interferogram after correcting the step height error and (d) the reconstructed spectrum before (green line) and after (red line) EMD

References

[1] Zhang C. Interference Imaging Spectroscopy. Science Press, 2010. 18.

[2] Zhang C, Xiangli B, Zhao B, et al. Optics Communications, 2002, 203(1-2): 21.

[3] Matallah N, Sauer H, Goudail F, et al. Proceedings of SPIE-the International Society for Optical Engineering, 2011, 8167(4): 816715-816715-13.

[4] Lucey P G, Wood M, Crites S T, et al. A LWIR Hyperspectral Imager Using a Sagnac Interferometer and Cooled HgCdTe Detector Array. SPIE Defense, Security, and Sensing, 2012. 83900Q-83900Q-8.

[5] Egorova L V, Anufriev A S. Journal of Optical Technology, 2013, 80(11): 703.

[6] Kudenov M W, Dereniak E L. Optics Express, 2012, 20(16): 17973.

[7] Pei L, Min H, Lv Q, et al. Optical System Design of the Snapshot Imaging Spectrometer Using Image Replication Based on Wollaston Prism. Society of Photo-Optical Instrumentation Engineers. Society of Photo-Optical Instrumentation Engineers (SPIE) Conference Series, 2015: 94440Y-94440Y-6.

[8] Pei L, Min H, Lv Q, et al. Optical System Design of the Snapshot Imaging Spectrometer Using Image Replication Based on Wollaston Prism. Society of Photo-Optical Instrumentation Engineers. Society of Photo-Optical Instrumentation Engineers (SPIE) Conference Series, 2015: 94440Y-94440Y-6.

[9] Wang W, Liang J, Liang Z, et al. Optics Letters, 2014, 39(16): 4911.

[10] Talghader J J, Gawarikar A S, Shea R P. Light Science & Applications, 2012, 1(8): e24.

[11] Blum O, Shaked N T. Light Science & Applications, 2015, 4(8): e322.

[12] Gao J, Liang Z, Liang J, et al. Applied Spectroscopy, 2016.

[13] Gonzalez R C, Woods R E, Eddins S L. Image Segmentation. In: R. Qiuqi (ed.) Digital Image Processing Using MATLAB, 2nd ed. Publication house of electronics industry, 2013. 212.

[14] Zhu W. Open CV Image Processing Programming Examples. Publishing House of Electronics Industry, 2016. 338.

[15] Richard Szeliski. Computer Vision: Algorithms and Applications. Tsinghua University Press, 2012. 160.

[16] Lowe D G, Lowe D G. International Journal of Computer Vision, 2004, 60(2): 91.

[17] Mikolajczyk K, Schmid C. IEEE Transactions on Pattern Analysis and Machine Intelligence, 2005, 27(10): 1615.

[18] Griffiths P R, De Haseth J A. Fourier Transform Infrared Spectrometry. 2nd ed. John Wiley & Sons, 2007. 167.

基于多级微反射镜的时空联合调制傅里叶变换成像光谱仪：原理及数据处理

高健华[1,2]，梁静秋[1]，吕金光[1*]，梁中翥[1]，秦余欣[1]，王维彪[1]

1. 中国科学院长春光学精密机械与物理研究所应用光学国家重点实验室，吉林 长春　130033
2. 中国科学院大学，北京　100049

摘　要　介绍了一种基于多级阶梯微反射镜的时空联合调制傅里叶变换成像光谱仪的原理及数据处理方法。仪器利用一块多级阶梯微反射镜取代传统迈克尔逊干涉仪中的动镜以实现静态干涉，通过摆镜扫描使目标物体成像在不同的子阶梯反射面上从而获得目标物体不同光程差的干涉信息。某一时刻，目标物体经摆镜与前置成像系统后在平面镜与多级阶梯微反射镜上形成两个一次像点，两个一次像点被平面镜和多级阶梯微反射镜反射之后经后置成像系统最终成像在探测器焦平面上。平面镜与多级阶梯微反射镜之间的高度差会使到达探测器的两束光的光程差不同，因此探测器焦平面上可以获得目标物体的二维空间信息及一维干涉信息。根据多级阶梯微反射镜参数及光学系统设计参数计算得到摆镜步进角度为 0.095°。利用实验获得的三维数据立方体进行了图像拼接与光谱复原。针对子阶梯反射镜存在宽度差异的问题，提出了一种基于极坐标霍夫变换的图像分割方法。为缓解拼接全景图中的间断线效应，将图像变换到 HSI 颜色空间并插值拟合其亮度分量后再变换回原空间。对拼接后的干涉图像进行了降维、去直流、寻址、切趾、相位校正、傅里叶变换及光谱分辨率增强等处理，完成了光谱复原工作。复原光谱分辨率为 194 cm^{-1}，优于设计指标(250 cm^{-1})。

关键词　傅里叶变换成像光谱仪；干涉图拼接；光谱复原；图像拼接

（**收稿日期**：2017-01-06，**修订日期**：2017-05-20）

*通讯联系人